Increasing throughput in cellular networks with higher-order sectorization

Howard Huang, Osama Alrabadi, John Daly, Dragan Samardzija,
Cuong Tran, Reinaldo Valenzuela, Susan Walker
Bell Labs, Alcatel-Lucent

Abstract—We study the impact of higher-order sectorization (up to 12 sectors per cell site) in cellular networks with low angle spread and a high density of users. Under ideal sector patterns (with no intersector interference), the mean throughput per site scales directly with S, the number of sectors per site. Fixing the number of antennas per site to be 12, higher-order sectorization with $S = 12$ and single-antenna transmission per sector is shown to achieve higher average throughput compared to a conventionally sectorized system with $S = 3$ and capacity-achieving multiuser MIMO transmission with $M = 4$ antennas per sector. A circular antenna array architecture is proposed for generating $S = 12$ sectors using fixed beamforming. Beams generated using an array prototype were measured in an anechoic chamber were shown to achieve a similar response as the one used in simulations, and the wind load improvement is a factor of 8 compared to the $S = 3, M = 4$ configuration.

I. INTRODUCTION

The downlink throughput in cellular networks can be increased by spatially multiplexing transmissions to multiple users using multiple antennas at the base. By reusing the spectral resources, these *multiuser (MU) MIMO* techniques [1] improve the spectral efficiency per site compared to single-antenna transmission. Alternatively, spectral efficiency per site can be increased through *sectorization* by partitioning each site radially into multiple sectors and reusing the spectral resources in each sector and across all sites. A sector is often implemented using a panel antenna which consists of multiple antenna elements enclosed within a single radome enclosure. The multiple elements are co-phased to create directional beams and to provide horizonal and vertical aperture gain.

Multiuser MIMO techniques can be used in conjunction with sectorization. For example, a cell site could be partitioned into 3 sectors, and for each sector, 4 panel antennas could be implemented for MU-MIMO. MU-MIMO provides up to roughly a factor of 4 improvement in throughput per sector compared to single-antenna transmission [1]. At high signal-to-interference-plus-noise ratio (SINR), this gain is achieved by multiplexing signals to 4 users. At low SINR, the gain could be achieved through multiplexing or by serving a single user but boosting its received power through coherent combining at the transmitter. The drawback of downlink MU-MIMO is that it requires coherent channel state information at the transmitter (CSIT). In TDD systems, CSIT could be obtained through uplink and downlink channel reciprocity, and in FDD systems, it could be obtained through uplink feedback.

Higher-order sectorization refers to the partitioning of cell sites into more than 3 sectors. If there is only a single transmit antenna per sector, the implementation of higher-order sectorization is simpler than MU-MIMO because CSIT is not required. Each mobile needs to indicate only the desired sector for service. Because the beamwidth of a sector is inversely proportional to the antenna aperture, narrower sectors for higher-order sectorization require larger antenna panels which place greater burdens on the supporting infrastructure to account for weight and wind load. Also, larger antennas are often visually more obtrusive.

In this paper, we show that higher-order sectorization using 12 sectors per site achieves similar performance to a conventional system with 3 sectors per site using MU-MIMO. Higher-order sectorization is much simpler to implement in terms of signal processing, and to address the problems associated with larger panel antennas, we propose a compact circular antenna array architecture for creating the sectors through fixed beamforming.

We present the system model in Section II, and we show how throughput per site scales directly with the number of sectors per under ideal sectorization in Section III. In Section IV, we show that similar gains can be achieved using non-ideal sector response, and we compare the performance of higher-order sectorization with MU-MIMO in Section V. The circular array architecture is presented in Section VI.

II. SYSTEM MODEL

We study the performance of a downlink cellular network consisting of hexagonal cell sites, each partitioned into $S = 3, 6,$ or 12 sectors. If we let B denote the total number of sectors in the network, the number of sites is B/S. Each sector is equipped with M directional transmit antennas whose broadside directions are shown in Figure 1. Each sector serves K users, each with N antennas. The downlink received signal by the kth user ($k = 1, \ldots, KB$) is:

$$\mathbf{x}_k = \sum_{b=1}^{B} \mathbf{H}_{k,b}^H \mathbf{s}_b + \mathbf{n}_k, \tag{1}$$

where $\mathbf{H}_{k,b}^H \in \mathbb{C}^{N \times M}$ is the MIMO channel between the kth user and the bth base ($b = 1, \ldots, B$), $\mathbf{s}_b \in \mathbb{C}^M$ is the transmitted signal from base b, and $\mathbf{n}_k \in \mathbb{C}^N$ is the thermal noise vector with distribution $\mathcal{CN}(\mathbf{0}_N, \mathbf{I}_N)$.

We assume the components of the channel $\mathbf{H}_{k,b}$ are i.i.d. Rayleigh with distribution $h_{k,b}^{(m,n)} \sim \mathcal{CN}(0, \alpha_{k,b}^2)$. The variance $\alpha_{k,b}^2$ depends on the distance-based pathloss, shadow
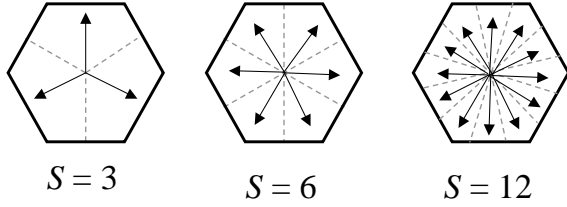
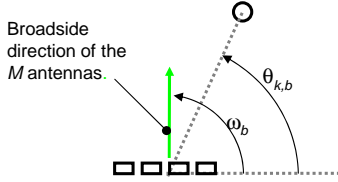Fig. 1. Broadside direction of sectorized antennas for $S = 3, 6, 12$ sectors per cell.

Fig. 2. The direction of user k with respect to the M antennas of sector b is given by $\theta_{k,b}$. The broadside direction of sector b is ω_b. These directions are measured with respect to the positive x-axis.

fading realization, and direction between user k and base b. It can be written as:

$$\alpha_{k,b}^2 = \left(\frac{d_{k,b}}{d_{\text{ref}}}\right)^{-\gamma} Z_{k,b} G_{k,b}, \tag{2}$$

where $d_{k,b}$ is the distance between user k and base b, d_{ref} is the reference distance with respect to which the pathloss is measured, γ is the pathloss exponent, $Z_{k,b}$ is the shadowing realization between user k and base b, and $G_{k,b}$ is the direction-based antenna response of the base antenna.

The antenna response is a function of the angular difference between the broadside direction of sector b (given by ω_b), and the direction of user k with respect to this sector (given by $\theta_{k,b}$). These variables are illustrated in Figure 2. Independent of S, the total transmit power per site is P, and this power is partitioned equally among the S sectors.

III. IDEAL SECTORIZATION

Under ideal sectorization, the sector response should be flat within the sector and zero outside the sector so there is no intersector interference. For a cell with S sectors, the ideal response would be:

$$G_{k,b}(\theta_{k,b} - \omega_b) = \begin{cases} 1 \text{ if } |\theta_{k,b} - \omega_b| \leq \frac{\pi}{S} \\ 0 \text{ if } |\theta_{k,b} - \omega_b| > \frac{\pi}{S} \end{cases} \tag{3}$$

In normalizing the antenna gain to be unity within the sector, we implicitly assume that the total transmit power per site is fixed and that the reduction in power per sector is offset by the gain achieved with the narrower beam pattern. Therefore, independent of S, the average received power by user k from base b is $P\alpha_{k,b}^2$ if the user lies within the sector beam width.

Let us consider the throughput performance of a cellular network with $S = 1$ omni-directional sector per site. A user is assigned to the base with the strongest average received signal

power, under the assumption that all bases transmit with power P. For user k ($k = 1, \ldots, KB$), the serving base, which we denote with index b^*, is given by $b^* = \arg\min_b \alpha_{k,b}^2$. This user receives signal power from its assigned base and interference power from the other $B - 1$ bases. Its *geometry* (defined as the average desired signal power divided by the average noise plus interference power) is

$$\Gamma_k := \frac{P\alpha_{k,b^*}^2}{1 + \sum_{b \neq b^*} P\alpha_{k,b}^2}, \tag{4}$$

where the noise is assumed to unit power. The geometry can be interpreted as the SINR if there is no Rayleigh fading. The corresponding capacity for this user, $\log_2(1+\Gamma_k)$, is a random variable that depends on its location and the shadowing realizations.

Under ideal sectorization with $S > 1$ and $M = 1$ antenna per sector, a given user is illuminated by exactly one sector per site. Therefore, because the received power from any site is independent of S, the geometry (4) is independent of S. It follows that the throughput distribution per sector is independent of S. As a corollary, the throughput statistics such as the mean throughput per sector are also independent of S. Under the assumption of $K = 1$ user per sector, the mean throughput per sector is independent of S, and the mean throughput *per site* scales directly with S.

IV. PARABOLIC SECTOR RESPONSE

In practice, the ideal sector response cannot be achieved, and each sector receives co-channel interference from other sectors belonging to the same site and from other sites. Figure 3 shows the ideal sector response for $S = 3$ and the response for a commercially available antenna. Over the main lobe, the non-ideal response is well-approximated using a parabolic function, and the intersector interference can be upperbounded using a flat response at -20dB. This analytic response, used for the spatial channel model (SCM) in standards simulations [2], is given by

$$G_{k,b}(\theta_{k,b} - \omega_b)(\text{dB}) = \max\left\{-12\left[\frac{(\theta_{k,b} - \omega_b)}{\Theta_{3\text{dB}}}\right]^2, -A_s\right\}, \tag{5}$$

where $\Theta_{3\text{dB}}$ is the 3dB beamwidth of the response A_s is the sidelobe level of the response, measured in dB. As with the ideal sector response, the response in (5) is normalized under the assumption of fixed transmit power per site. Figure 3 also shows the parabolic responses for $S = 3, 6, 12$ sectors using the parameters in Table I. The parameters are chosen so that the beamwidth and sidelobe levels scale with S: by doubling S, the beamwidth is halved, and the sidelobe levels drop by 3dB.

Assuming a pathloss coefficient of $\gamma = 3.76$, shadow fading with standard deviation 8dB, and reference SNR 30 dB (which for unit variance noise is equivalent to $P = 1000$), Figure 4 shows the cumulative distribution function (CDF) of the geometry (4) for $S = 1, 3, 6, 12$ sectors per site with $M = 1$ antenna per sector. (The reference SNR measures the average SNR at the cell edge when a single base transmits with

full power [3]. Our assumption of a 30dB reference SNR corresponds to the interference-limited regime.) Compared to $S = 1$ whose geometry is unbounded because a user can be arbitrarily close to the serving base, the geometry for $S \geq 3$ is limited as a result of interference from other sectors belonging to the same site. For high SNR ($P \gg 1$), the maximum geometry is $\left[10 \log_{10}(A_S)\right]/(S - 1)$, for $S = 3, 6, 12$ and where A_S is given by Table I. Because of the scaling of the parameters in Table I, the distribution of the geometry for a user k at a given angle $|\theta_{k,b^*} - \omega_{b^*}| \leq \pi/S$ with respect to its serving sector b^* under $S = 3$ will be similar to the distribution at the angle $(\theta_{k,b^*} - \omega_{b^*})/2$ under $S = 6$ and at the angle $(\theta_{k,b^*} - \omega_{b^*})/4$ under $S = 12$. Therefore the CDF of the geometry (unconditioned on the angle) will be similar for $S = 3, 6, 12$.

The rate achievable by user k assigned to base b^*, given the Rayleigh channel realizations, is:

$$\log_2\left(1 + \frac{P|h_{k,b^*}|^2}{1 + \sum_{b \neq b^*} P|h_{k,b}|^2}\right), \qquad (6)$$

If a single user is served per sector, the distribution of the rate per user is equivalent to the distribution of the throughput per sector. Because the geometry distributions for $S = 3, 6, 12$ are similar, the resulting throughput distributions *per sector* are also similar. A throughput realization *per site* is obtained by summing the throughput across S co-located sectors for a given placement of users and channel realizations, and the resulting CDF is shown in the bottom subfigure of Figure 5. As a result of the central limit theorem and the fact that the throughput realizations per sector are independent, the throughput distribution per site becomes more Gaussian as S increases. The mean throughput roughly doubles in going from $S = 1$ to 3. Because the throughput per sector is largely independent of S (for $S \geq 3$), the mean throughput per site doubles in going from $S = 3$ to 6, and from $S = 6$ to 12. Therefore as a result of the judiciously parameterized antenna pattern, the mean throughput under higher-order sectorization with parabolic antenna patterns scales linearly with $S \geq 3$, as was observed for the ideal sectorization case.

The sector responses given by (5) and Table I assume the channel has zero angle spread. As the angle spread increases, the effective sector beamwidth increases, resulting in additional intersector and intercell interference. The equivalent response can be obtained by convolving (in the angular domain) the channel's power azimuth spectrum (PAS) with the zero-angle-spread response in (5) [4]. The power azimuth spectrum of a typical urban macrocellular channel can be modeled as a Cauchy-Lorenz distribution with an RMS angle spread of $\phi = 8\pi/180$ radians [5]. The relatively narrow angle spread is due to the fact that the base station antennas are higher than the surrounding scatterers. Figure 6 shows the resulting antenna responses for $S = 3, 6, 12$ sectors. Because the PAS is relatively narrow compared to the baseline $S = 3$ response in Figure 3, the resulting convolved response is similar to the baseline response. However, the PAS is wide compared to the $S = 12$ baseline response, and the resulting convolved response is significantly wider than the baseline response.
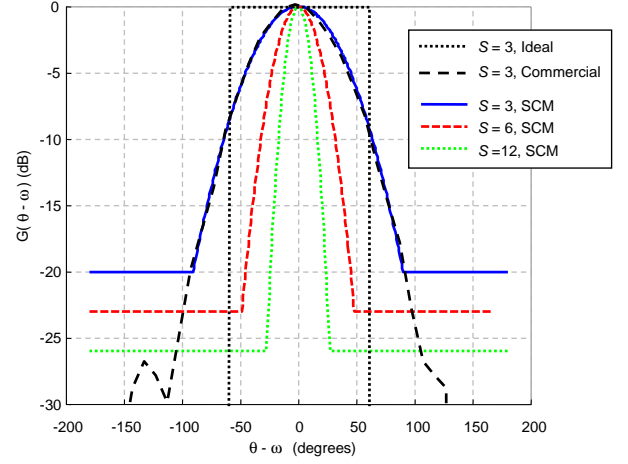

Fig. 3. Parabolic responses for $S = 3, 6, 12$ sectors per site, given by (5) and parameters in Table I

Number of sectors per cell (S)	$\Theta_{3\mathrm{dB}}$	A_s
3 sectors	$(70/180)\pi$	-20 dB
6 sectors	$(35/180)\pi$	-23 dB
12 sectors	$(17.5/180)\pi$	-26 dB

TABLE I
ANTENNA PATTERN PARAMETERS

Figure 7 shows the mean throughput performance versus the RMS angle spread. The performance of higher-order sectorization is more sensitive because for a fixed angle spread, there is more interference. In going from zero to ten degrees angle spread, the throughput for $S = 12$ is reduced by almost 40% whereas the throughput for $S = 6$ is reduced by only 20%. However, the absolute throughput for $S = 12$ is still superior and is over twice the throughput of conventional sectorization $S = 3$. As the angle spread increases beyond 40 degrees, there is very little throughput advantage in using $S = 12$ compared to $S = 6$ sectors.
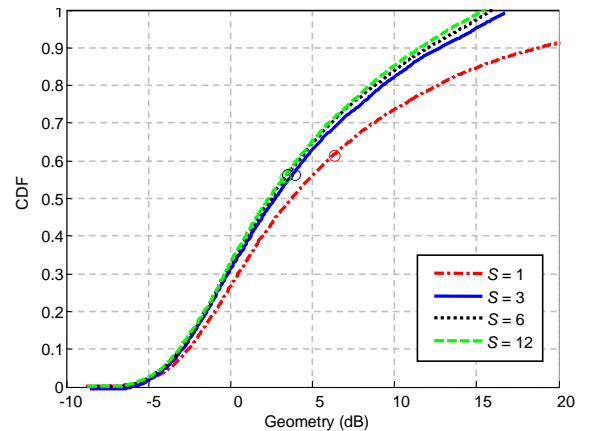

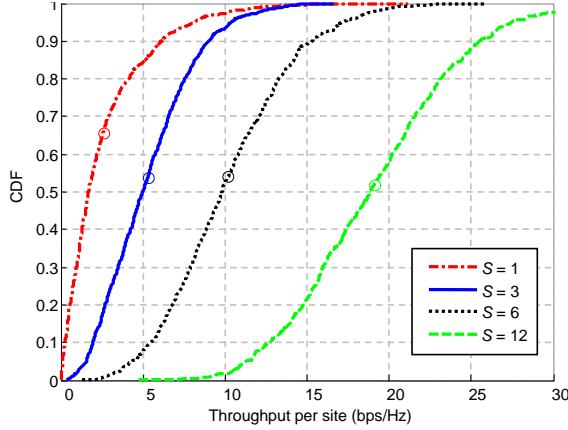Fig. 4. CDF of geometry (4) , parameterized by S, the number of co-channel sectors per site.

Fig. 5. CDF throughput per site (6), based on the geometries from Figure 4. Mean throughput per site approximately doubles in going from $S = 3$ to 6 sectors and again from $S = 6$ to 12 sectors.
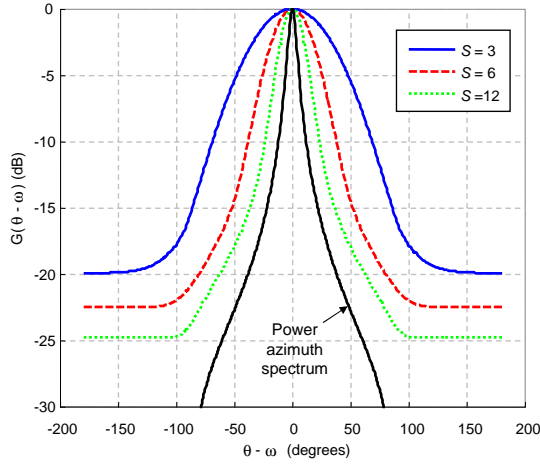

Fig. 6. Sector responses for $S = 3, 6, 12$ sectors per site obtained by convolving the power azimuth spectrum (for 8 degree angle spread) with the parabolic response in Figure 3.
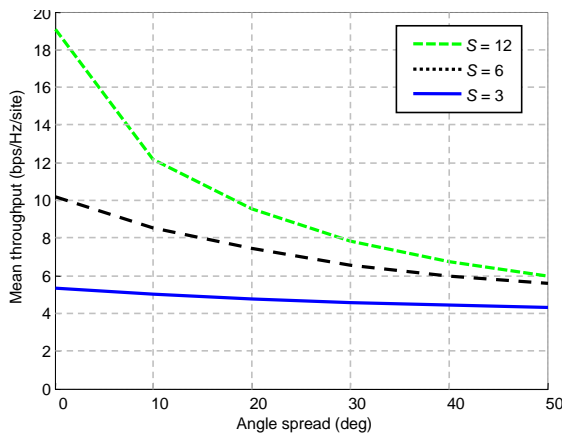

Fig. 7. Mean throughput per site versus RMS angle spread, using the sector parameters in Table I. As the angle spread increases, the effective sector response becomes wider, resulting in additional interference and degraded performance. For a given angle spread, performance degradation for narrower sectors is more severe.

V. FIXED NUMBER OF ANTENNAS PER SITE

We have just shown that higher-order sectorization increases the throughput per site as the number of sectors and antennas per site increase. In this section we present a more fair comparison where the number of antennas per site is fixed as the sectorization order increases. We fix the number of antennas per site to be 12 and consider $S = 3, 6, 12$. The number of antennas per sector is $M = 12/S$, and we let the number of users per sector be $K = M$. Each user is equipped with $N = 2$ antennas. We use a parabolic sector response (5) with parameters given by Table I. The system parameters are summarized in Figure 8.

For $S = 3$ and 6, the multiple antennas in each sector have the same broadside direction as shown in Figure 1. By accounting for the intercell and intersector interference as noise, the channel for users associated with a given sector can be modeled as a broadcast channel with M antennas and $K = M$ users. For a given set of user locations and channel realizations, we determine the rate vector $\mathbf{R} := [R_1, \ldots, R_K]$ belonging to the broadcast channel rate region $\mathcal{C}(\mathbf{H}_1^H, \ldots, \mathbf{H}_K^H, P)$ such that the sum of log rates is maximized:

$$\mathbf{R}^* = \arg\max_{\mathbf{R} \in \mathcal{C}} \sum_{k=1}^K \log R_k. \tag{7}$$

This rate vector $\mathbf{R}^* \in \mathcal{C}$ is proportionally fair in the sense that for any $\mathbf{R} \in \mathcal{C}$, $\sum_k (R_k - R_k^*)/R_k^* \leq 0$ [6]. The proportional fair vector in (7) can be obtained numerically using an iterative gradient scheduling algorithm [7] where, on each iteration, the weighted sum rate maximizing rate vector can be found using a gradient-based optimization [8]. The proportional fair rate vector is achieved using MU-MIMO transmission based on dirty paper coding (DPC) and linear precoding.

For $S = 12$ sectors, each sector transmits with $M = 1$ antenna, and each user demodulates its desired signal with maximal ratio combining. The achievable rate is over this single-user SIMO channel is:

$$\log_2\left(1 + \frac{P\|\mathbf{h}_{k,b^*}\|^2}{1 + \sum_{b \neq b^*} P\frac{|\mathbf{h}_{k,b^*}^H \mathbf{h}_{k,b}|^2}{\|\mathbf{h}_{k,b^*}\|^2}}\right). \tag{8}$$

The user rate distribution is obtained using Monte Carlo simulations over random channel realizations. Letting R be the random variable representing the user rate, we compute the normalized peak user rate $SK \times \{\arg_z [\Pr(R \leq z)] = 0.9\}$, the normalized cell-edge user rate $SK \times \{\arg_z [\Pr(R \leq z)] = 0.1\}$, and the normalized mean user rate $SK \times \mathbb{E}(R)$. The cell-edge and peak rates are normalized to make easier comparisons with the mean throughput per site, which we note is equivalent to the normalized mean user rate.

The performance for the three system options is summarized in Figure 9. For a fixed number of antennas per site, $S = 12$ achieves the highest normalized peak rate and mean throughput per site. Its cell-edge rate is competitive with the other options. As a first-order approximation, all three options allow the spectral resources to be reused 12 times in each site, and the superior performance for $S = 12$ is a result of the sector
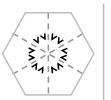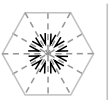
Fig. 8. Parameters for downlink system simulations, 12 antennas per site, with $S = 3, 6$ or 12 sectors per site. Capacity-achieving MU-MIMO transceivers are used for $S = 3$ and $S = 6$. Single-user SIMO is used for $S = 12$.
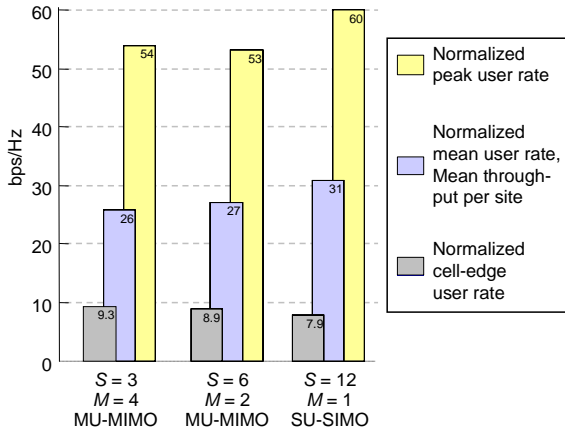

Fig. 9. Performance for system options shown in Figure 8, for 12 antennas per site and zero-degree angle spread. Higher-order sectorization with $S = 12$ achieves the highest peak rate and mean throughput.

Structure	Force (normalized)
Circular array	1.0
$S = 3, M = 4$	4.2
$S = 6, M = 2$	13
$S = 12, M = 1$	25

TABLE II

NORMLIZED WIND LOADING FORCE FOR ANTENNA ARRAY CONFIGURATIONS GIVEN IN FIGURE 8 AND THE CIRCULAR ARRAY SHOWN IN FIGURE 11.

with approximately 0.5 λ inter-element spacing and a diameter of 3.8 λ. The carrier frequency is 2.45 GHz, and the array diameter is approximately 21 inches. The array size is very compact compared to a conventional deployment with $S = 3$ and diversity-spaced antennas where the site array consists of an equilateral triangular platform where each side has length up to 10 λ.

Each element of the circular array is mildly directional and has an azimuthal beamwidth of about 90 degrees. Twelve simultaneous fixed beams can be generated as shown in Figure 12. Each beam is created by weighting the complex amplitude of 7 adjacent elements, such that for the beam pointing in one of 12 hourly clock directions is formed using the 7 elements centered around that direction. If all beams are activated, each element contributes to either 3 or 4 beams.

Beamforming weights were determined based on a Chebyshev filter design with tapered weights, and the resulting beam pattern response measured in an anechoic chamber is shown in Figure 13. The measured response very closely matches the main beam of the SCM sector response using the parameters for the $S = 12$-sector in Table I, and the sidelobe characteristics are near or below -26dB. By activating 12 beams with this pattern, the resulting throughput performance using the prototype beam pattern should be similar to the $S = 12$ performance in Figure 9.

A first-order approximation of the wind loading for antenna arrays can be made using aerodynamic theory [9] and an industry standard TIA-222-G for telecommunication structures [10]. Under reasonable simplifying assumptions (steady incompressible flow, no-ice condition, ignore effects of mounting brackets and cables, unity gust-effect factor) and a fixed wind velocity, the wind load force is proportional to the product of the drag coefficient and the effective projected area (EPA), defined as the exposed area to the wind at a particular angle multiplied by the drag coefficient. The drag coefficient values used from the standard [10] were 0.5 for the circular array and 1.4 for the commercial arrays with single-polarized panel-antenna implementations. As a result of the lower drag coefficient and lower exposed area, the circular array achieves superior wind loading performance compared to the panel implementations, as shown in Table II.

response parameters. (The performance would be even better using ideal sectorization.) SIMO transmission under $S = 12$ is very simple to implement compared to MU-MIMO because it does not require CSIT nor complex DPC, and it is very robust to channel mismatch.

VI. CIRCULAR ARRAY IMPLEMENTATION

Higher-order sectorization can be implemented using panel antennas. However, because the panel width scales proportionally with the reciprocal of the beam width, higher order sectorization requires additional, wider panel antennas. These panels place greater burdens on the supporting infrastructure to account for the weight and wind load. To address the problems associated with larger panel antennas, we propose to implement higher-order sectorization through electronic beamforming using a compact circular antenna array architecture.

To guide the beam pattern design, we study the average throughput performance for $S = 3, 6, 12$ sectors as a function of a general parabolic beam pattern (5). Figure 10 shows the performance as a function of the beamwidth $\Theta_{3\mathrm{dB}}$, parameterized for sidelobe levels $A_s = -20$dB and -26dB. Throughput is maximized using $S = 12$ sectors, $\Theta_{3\mathrm{dB}} = 15$ degrees, and a sidelobe level of $A_s = -26$dB, providing motivation to design beams that target the $S = 12$-sector parameters in Table I.

A prototype for the circular array is shown in Figure 11. It consists of 24 vertical antenna elements, arranged in a cylinder

VII. CONCLUSIONS

We have shown that, in densely populated cells with low angle spread, higher-order sectorization with $S = 12$ sectors per site using single-antenna transmission achieves comparable performance with conventional $S = 3$-sector sites using opti-
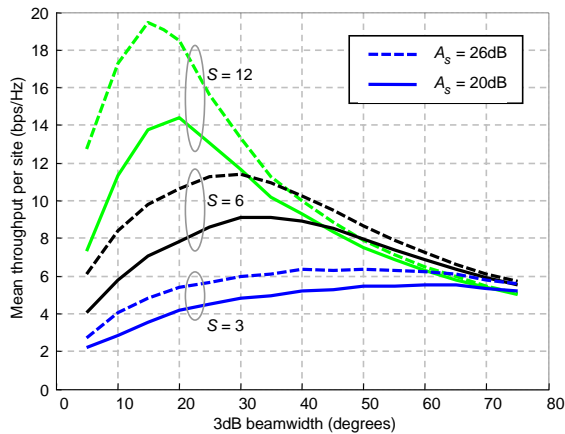
Fig. 10. Mean throughput per site versus sector beamwidth $\Theta_{3\text{dB}}$ for $S = 3, 6, 12$ sectors per site, parameterized by the sidelobe levels A_s. Zero-degree angle spread is assumed. For the given sidelobe levels in Table I, the throughput performance is nearly optimal for the corresponding beamwidths given by the table.
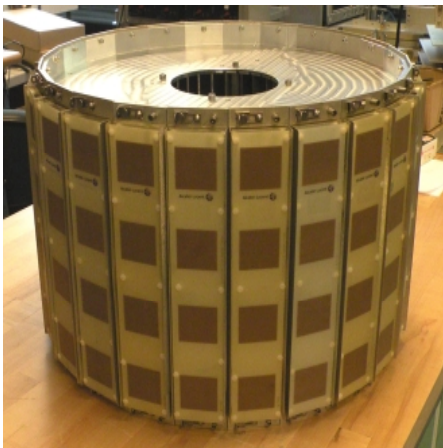

Fig. 11. Prototype for circular array designed for a 2.45GHz carrier frequency. The elements have a spacing of 0.55 λ, and the diameter is approximately 21 inches.
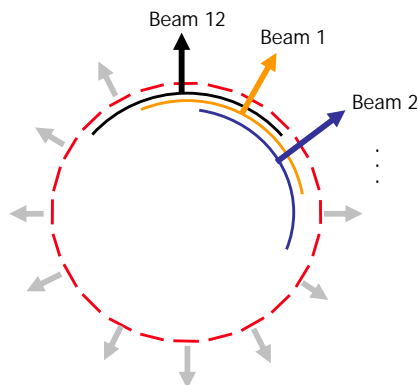

Fig. 12. Implementation of 12 fixed beams using a circular array with 24 elements.
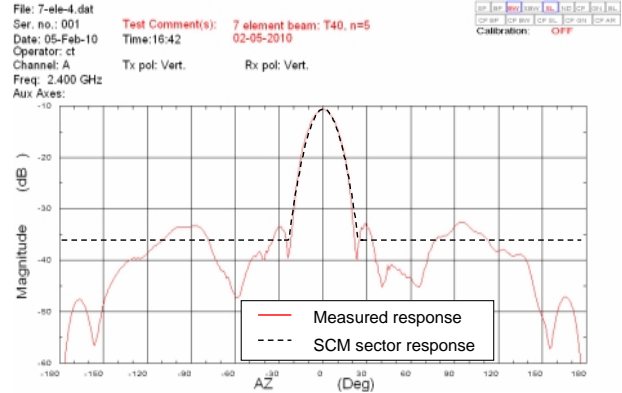

Fig. 13. Measured sector response of the circular array prototype compared to the analytical response from (5) for $S = 12$.

mal capacity-achieving multiuser MIMO transmission. Higher-order sectorization with necessary beamwidth and sidelobe characteristics can be implemented using a circular antenna array to generate fixed beams through beamforming. The beam characteristics of this array were verified through measurements in an anechoic chamber. In addition, the circular array has superior wind loading characteristics compared to conventional panel-antenna implementations.

For the throughput results, we have assumed that there is a sufficiently high density of users so that all sectors are occupied with active users. This condition may not be met in practice if there is a non-uniform distribution of users. In this case, power could potentially be shifted away from non-active sectors to increase the range of sectors with active users. The circular array architecture could also implement adaptive beams which track the position of users based on second-order channel statistics.

REFERENCES

[1] D. Gesbert, M. Kountouris, R. W. Heath, C.-B. Chae, and T. Salzer, "Shifting the MIMO paradigm," *IEEE Signal Processing Magazine*, vol. 24, no. 5, pp. 36–46, 2007.
[2] G. Calcev, D. Chizhik, B. Goransson, S. Howard, H. Huang, A. Kogiantis, A. F. Molisch, A. L. Moustakas, D. Reed, and H. Xu, "A wideband spatial channel model for system-wide simulations," *IEEE Transactions on Vehicular Technology*, vol. 56, no. 2, pp. 389–403, 2007.
[3] H. Huang, C. Papadias, and S. Venkatesan, *MIMO Communication for Cellular Networks*. Springer Publishing, 2011.
[4] A. Papoulis, *The Fourier integral and its applications*. McGraw Hill, 1987.
[5] D. Chizhik and J. Ling, "Propagation over clutter: Physical stochastic model," *IEEE Transactions on Antennas and Propagation*, vol. 56, no. 4, pp. 1071–1077, 2008.
[6] S. Venkatesan, "Coordinating base stations for greater uplink spectral efficientcy: Proportionally fair user rates," *IEEE International Symposium on Personal, Indoor and Mobile Radio Communications*, 2007.
[7] A. L. Stolyar, "On the asymptotic optimality of the gradient scheduling algorithm for multiuser throughput allocation," *Operations Research*, vol. 53, no. 1, pp. 12–25, January-February 2005.
[8] H. Viswanathan, S. Venkatesan, and H. Huang, "Downlink capacity evaluation of cellular networks with known-interference cancellation," *IEEE Journal on Selected Areas in Communications*, vol. 21, pp. 802–811, 2003.
[9] J. D. Anderson, *Fundamentals of Aerodynamics*. McGraw-Hill, 1991.
[10] *ANSI/TIA-222-G-2005 Structural standards for antenna supporting structures and antennas*, Telecommunications Industry Association Std.